

Weierstraß-Institut für Angewandte Analysis und Stochastik

im Forschungsverbund Berlin e.V.

Preprint

ISSN 0946 – 8633

External cavity modes in Lang-Kobayashi and traveling wave models

Mindaugas Radziunas¹ , Hans-Jürgen Wünsche² ,

Bernd Krauskopf³ , Matthias Wolfrum¹

submitted: 21 March 2005

¹ Weierstraß-Institut
für Angewandte Analysis und Stochastik
Mohrenstrasse 39
D – 10117 Berlin
Germany
E-Mail: radziunas@wias-berlin.de,
wolfrum@wias-berlin.de

² Humboldt-Universität zu Berlin
Institut für Physik
Newtonstr. 15
D – 12489 Berlin
Germany
E-Mail: wuensche@physik.hu-berlin.de

³ Dept. of Engineering Mathematics
University of Bristol
Bristol BS8 1TR
United Kingdom
E-Mail: b.krauskopf@bristol.ac.uk

No. 1111

Berlin 2006



2000 *Mathematics Subject Classification.* 35B60 78A60 37M20 37N20.

Key words and phrases. Lang-Kobayashi model, Traveling wave model, feedback laser, cavity modes .

2003 *Physics and Astronomy Classification Scheme.* 42.55.Px 42.65.Sf 42.60.Da 02.30.Jr 02.30.Ks 02.30.Mv.

Supported by the DFG Research Center MATHEON "Mathematics for key technologies".

Edited by
Weierstraß-Institut für Angewandte Analysis und Stochastik (WIAS)
Mohrenstraße 39
10117 Berlin
Germany

Fax: + 49 30 2044975
E-Mail: preprint@wias-berlin.de
World Wide Web: <http://www.wias-berlin.de/>

Abstract

We investigate a semiconductor laser with delayed optical feedback due to an external cavity formed by a regular mirror. We discuss similarities and differences of the well-known Lang-Kobayashi delay differential equation model and the traveling wave partial differential equation model. For comparison we locate the continuous wave states in both models and analyze their stability.

1 Introduction

In this paper we compare two approaches to modeling a semiconductor laser with conventional optical feedback (COF), where the laser is subject to delayed optical feedback due to an external cavity (EC) that is formed by a regular mirror at a fixed distance from the laser. The first approach is to model the system with the Lang-Kobayashi (LK) rate equations [1], which are delay differential equations (DDEs) for the electric field and the inversion inside the laser. The second approach is to use a traveling wave (TW) model [2, 3], where the system is described by partial differential equations (PDEs) for the optical waves that counter-propagate along the longitudinal axis of the laser.

Delay differential equation models, such as the LK equations have been shown to be powerful tools for simulation and analysis of the dynamics of lasers with different kinds of optical feedback. In addition to the case of COF considered here, lasers with filtered feedback, phase-conjugate feedback, and two lasers with a delayed coupling have recently been investigated by means of LK-type models [4]. In such DDE models the optical field is described by a complex amplitude, which means that the laser's length and the spatial distribution of the fields within the laser are not resolved. The influence of the delayed feedback is modeled by a driving force on the optical field in the lasing section.

For the COF laser this force is given by the delayed field multiplied by a complex feedback rate that describes the amplitude and phase of the light that re-enters the laser. Originally the LK equations were developed for the case of large delays and weak feedback. For shorter delay times and higher coupling strengths [5], the question arises whether this modeling approach is still justified.

The alternative is to describe a laser with optical feedback with a travelling wave PDE model that includes the spatial (longitudinal) distribution of the fields. This approach is more frequently used to describe the dynamics of integrated multisection lasers, where the sections are short (on the order of the length of the laser).

The complex amplitudes of the counter-propagating waves can be mutually coupled by Bragg gratings (if present). The TW model is then completed by reflectivity conditions at the edges of the laser. The counter-propagating waves are coupled through the standard carrier rate equation in the active section.

For the COF laser as discussed here (see Fig. 1) the TW model[6, 7] has the following properties. In the passive EC the optical fields remain uncoupled, which allows one to calculate the fields in the EC explicitly. The influence of the EC on the laser then enters as a delayed feedback term in the boundary condition of the laser section. There is an associated complex feedback strength, which is defined by the field losses and the phase shift within the EC, as well as by the field reflectivity at the outer EC facet.

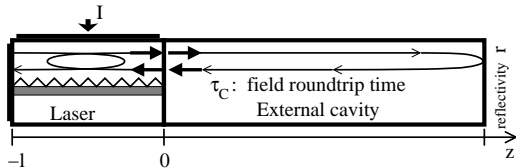


Figure 1: Scheme of a semiconductor laser with conventional optical feedback from an external cavity.

We present here a direct comparison of the continuous wave solutions and their stability properties, which are referred to in the LK model as the *external cavity modes* (ECMs) and in the TW model as the *compound cavity modes* (CCMs). After a suitable normalization, we are able to show that the equations determining the ECMs in the LK model can be understood as a local approximation for similar, but more complicated equations for the CCMs in the TW model. In particular, this allows us to relate the feedback rate of the LK model to the feedback strength used in the TW model.

2 Mathematical Models

In this section we give the formulations of the LK and the TW models for the COF laser device in Fig. 1.

2.1 Lang-Kobayashi model

Lang and Kobayashi have suggested[1] that single-mode lasers with weak feedback from a long external cavity can be modeled by modified rate equations. Here the laser length can be neglected and the optical fields are represented by the complex function $E(t)$. In dimensionless form the LK model can be written as

$$\begin{aligned} \dot{E}(t) - (1 + i\alpha_H)NE(t) &= \eta e^{i\psi} E(t - \tau_c), \\ \dot{N}(t) &= \varepsilon (J - N(t) - (2N(t) + 1)|E(t)|^2). \end{aligned} \tag{1}$$

Here N is the dimensionless excess carrier number (inversion), α_H is the linewidth enhancement (or Henry) factor, ε represents the ratio of photon and carrier life

times, and J is the excess pumping rate. The feedback term contains the delay time τ_c , the (real) feedback rate η , and the feedback phase ψ .

2.2 Traveling wave model

We take into account the spatio-temporal distributions of the electrical field, both in the laser and in the external cavity. Throughout we assume that the solitary laser is operating at single mode, that is, all other longitudinal modes remain well suppressed even in the presence of optical feedback. In this case we can neglect gain dispersion[3]. Under these assumptions the TW model[2] can be used to describe the dynamics of our laser device.

The TW model considers the evolution of the pair of slowly varying complex counter-propagating optical fields $\Psi(\tilde{z}, \tilde{t}) = (\Psi^+, \Psi^-)^T$ and the spatially averaged carrier density $n(\tilde{t})$. By proper scaling, $|\Psi(\tilde{z}, \tilde{t})|^2 = |\Psi^+|^2 + |\Psi^-|^2$ and $\langle |\Psi(\tilde{t})|^2 \rangle_L$ are the local and the spatially averaged photon densities in the laser. Taking into account the loss and the phase shift of the fields in the external cavity, we can write the TW model for our laser as

$$\begin{aligned} \frac{-i}{v_g} \frac{\partial}{\partial \tilde{t}} \Psi^\pm(\tilde{z}, \tilde{t}) &= \left(\pm i \frac{\partial}{\partial \tilde{z}} - \beta(n) \right) \Psi^\pm(\tilde{z}, \tilde{t}) - \bar{\kappa} \Psi^\mp(\tilde{z}, \tilde{t}), & \tilde{z} \in [-\bar{l}, 0], \\ \beta(n) &= \frac{i - \alpha_H}{2} g'(n(\tilde{t}) - n_{tr}) + \delta - \frac{i\alpha}{2}; \\ \Psi^+(-\bar{l}, \tilde{t}) &= 0, & \Psi^-(0, \tilde{t}) &= r K e^{i\varphi} \Psi^+(0, \tilde{t} - \bar{\tau}_c), \\ \frac{d}{d\tilde{t}} n(\tilde{t}) &= \frac{I}{e l \sigma} - \frac{n(\tilde{t})}{\tau} - v_g g'(n(\tilde{t}) - n_{tr}) \langle |\Psi(\tilde{t})|^2 \rangle_L. \end{aligned} \quad (2)$$

The real parameters v_g , g' , n_{tr} , and α are the group velocity, the differential gain, the transparency carrier density, and the internal absorption of the fields in the laser, respectively. The complex factor $\bar{\kappa}$ allows us to model distributed feedback (DFB) lasers; it represents the index ($\Re m \bar{\kappa}$) and the loss ($\Im m \bar{\kappa}$) coupling of the fields. The selection of the wavelength detuning factor δ allows us to shift the operation wavelength (frequency) with respect to the central wavelength λ_0 ¹. The parameters φ and K denote the 2π -periodic field phase shift and the field amplitude transmission factor during the field roundtrip in the EC. The complex number r is the non-vanishing reflectivity of the field *amplitude* at the outer edge of the EC. The parameters \bar{l} and $\bar{\tau}_c$ denote the laser length and the field roundtrip time in the EC in the nonscaled model. Finally, I , σ , e , τ are the injected current, the crosssection area of the active zone, the electron charge, and the carrier life time, respectively.

We normalize the TW model (2) by scaling the coordinates and the functions according to

$$\begin{aligned} z &:= g'(n_{\text{ref}} - n_{tr}) \tilde{z}, & t &:= v_g g'(n_{\text{ref}} - n_{tr}) \tilde{t}, \\ N(t) &:= \frac{n(\tilde{t}) - n_{\text{ref}}}{2(n_{\text{ref}} - n_{tr})}, & E(z, t) &:= \sqrt{\frac{v_g g' \tau}{2}} \Psi(\tilde{z}, \tilde{t}), \end{aligned}$$

and by introducing the dimensionless parameters

$$l = g'(n_{\text{ref}} - n_{tr}) \bar{l}, \quad \tau_c = v_g g'(n_{\text{ref}} - n_{tr}) \bar{\tau}_c, \quad \varepsilon \stackrel{\text{def}}{=} \frac{1}{v_g \tau g'(n_{\text{ref}} - n_{tr})},$$

¹The related optical frequency is $2\pi c_0 / \lambda_0$, where c_0 denotes the speed of light in vacuum.

Table 1: Parameters and their values.

nonscaled parameters			dimensionless and scaled parameters		
central wavelength	λ_0	1.57 μm	group velocity factor	c_0/v_g	3.6
effective differential gain	g'	9 10^{-17}cm^2	Henry factor	α_H	4
length of DFB section	\bar{l}	200 μm	scaled length of DFB section	l	1.8
roundtrip time in EC	$\bar{\tau}_c$	12 ps	scaled roundtrip time in EC	τ_c	9
index coupling coefficient	$\Re e \bar{\kappa}$	130 cm^{-1}	scaled index coupling	$\Re e \kappa$	2.6
loss coupling coefficient	$\Im m \bar{\kappa}$	5 cm^{-1}	scaled loss coupling	$\Im m \kappa$	0.1
inverse carrier life time	τ	4/3 ps	photon / carrier life time ratio	ε	0.001
current injection	I	43.26 mA	excess pumping rate	J	1
cross-section area of AZ	σ	0.45 μm^2	facet reflectivity amplitude	$ r $	0.978
transparency carrier density	n_{tr}	1 10^{18}cm^{-3}	facet reflectivity argument	$\arg(r)$	1.248 π
reference carrier density	n_{ref}	2 10^{18}cm^{-3}	transmission amplitude in TW	K	2 η
wavelength detuning	δ	-10 cm^{-1}	feedback rate amplitude in LK	η	$K/2$
internal absorption	α	23.8 cm^{-1}	feedback phases	$\phi = \varphi$	

$$\kappa \stackrel{\text{def}}{=} \bar{\kappa} \bar{l}, \quad \xi_0 \stackrel{\text{def}}{=} \left(\frac{1+i\alpha_H}{2} g' (n_{\text{ref}} - n_{tr}) - \frac{\alpha}{2} - i\delta \right) \bar{l},$$

$$J \stackrel{\text{def}}{=} \frac{I - I_{\text{ref}}}{2(I_{\text{ref}} - I_{tr})}, \quad \text{where} \quad I_j \stackrel{\text{def}}{=} \frac{e \bar{l} \sigma n_j}{\tau}, \quad j = \text{ref, tr.}$$

Now the TW model can be written in dimensionless form as

$$\begin{aligned} \frac{\partial}{\partial t} \begin{pmatrix} E^+ \\ E^- \end{pmatrix} (z, t) &= H(N) \begin{pmatrix} E^+ \\ E^- \end{pmatrix}, \quad z \in (-l, 0), \\ E^+(-l, t) &= 0, \quad E^-(0, t) = r K e^{i\varphi} E^+(0, t - \tau_c), \\ H(N) &\stackrel{\text{def}}{=} \begin{pmatrix} -\partial_{z^+} + (1 + i\alpha_H)N + \xi_0/l & -i\kappa/l \\ -i\kappa/l & \partial_{z^+} + (1 + i\alpha_H)N + \xi_0/l \end{pmatrix}, \\ \frac{d}{dt} N(t) &= \varepsilon (J - N - (2N + 1) \langle |E|^2 \rangle_L). \end{aligned} \quad (3)$$

In the following, we focus on the comparison between the nondimensional equations (1) and (3) of the Lang-Kobayashi and TW models, respectively. For notational simplicity, $E(z, t)$ will be used to represent the optical amplitudes in both cases. However, it is important to keep in mind that the $E(z, t)$ is actually independent of z in the Lang-Kobayashi model, while it represents the two component vector $(E^+(z, t), E^-(z, t))^T$ in the TW model.

3 Cavity modes

A cavity mode (CM) or a continuous wave (CW) state of the COF laser device is a solution of the model equations given by

$$(E(z, t), N(t)) = (E_s(z) e^{i\omega_s t}, N_s), \quad (4)$$

where $E_s(z)$ and N_s represent a time-independent complex optical field and a real carrier number, and the real constant ω_s is an angular frequency. In both of our models the field equations are linear in the laser with respect to the field function

E . This means that the field equations determine the real pairs (ω_s, N_s) , while the amplitude of E_s can be found later from the balance of the carrier rate equation.

In order to determine the possible CMs, ansatz (4) is inserted into the respective model equations. Following [6], the result is written as

$$\mathcal{G}(\omega, N) = \zeta e^{i\phi} e^{-i\omega\tau_c} \quad (5)$$

in both cases. Here, $\mathcal{G}(\omega, N)$ and the right-hand side of Eq. (5) represent the response of the laser and of the EC to the same monochromatic field. The complex function $\mathcal{G}(\omega, N)$, the effective coupling parameter ζ and phase ϕ depend on the model. Before specifying them, we first discuss this equation in general.

In the absence of the feedback ($\zeta = 0$) the roots (ω_0, N_0) of the function $\mathcal{G}(\omega, N)$ determine the CW states of the solitary laser. For nonzero feedback, Eq. (5) suggests an easy way to locate the CMs, or branches of CMs when the feedback parameters ζ or ϕ are changed. Namely, these branches in the (ω, N) -projection can be represented by level curves of the functions²

$$\tilde{\zeta}(\omega, N) = |\mathcal{G}(\omega, N)|, \quad \tilde{\phi}(\omega, N) = \arg(\mathcal{G}(\omega, N)) + \omega\tau_c \pmod{2\pi}. \quad (6)$$

After defining the complex function $\mathcal{G}(\omega, N)$ and fixing the parameters ζ and ϕ , one can trace these level curves numerically³ (see, *e.g.*, the solid and dashed curves in Fig. 2). The CMs of our system are then given by the intersection points (ω, N) of the level curves of both these functions (the black dots in Fig. 2).

Any pair (ω, N) corresponds to some CM of the laser with the feedback amplitude $\tilde{\zeta}(\omega, N)$ and phase $\tilde{\phi}(\omega, N)$. Without additional efforts we record changes of the amplitude $\zeta = \tilde{\zeta}(\omega, N)$ (or phase $\phi = \tilde{\phi}(\omega, N)$) when we tune (ω, N) along the computed level curve of $\tilde{\phi}$ (or $\tilde{\zeta}$) in the (ω, N) -projection. We distinguish possibly stable node (*mode*) CMs and unstable saddle-type (*antimode*) CMs. Pairs of *modes* and *antimodes* are created or destroyed at folds of branches (saddle-node bifurcations). This creation or disappearance of pairs of CMs can be recognized in the (ω, N) -projection: it happens at those (ω, N) , where level curves of $\tilde{\zeta}(\omega, N)$ and $\tilde{\phi}(\omega, N)$ are touching each other. That is, the real equation

$$\partial_\omega \tilde{\phi} \partial_N \tilde{\zeta} = \partial_\omega \tilde{\zeta} \partial_N \tilde{\phi} \quad \Leftrightarrow \quad 0 = \mathcal{F}(\omega, N) \stackrel{def}{=} \Re e(\partial_N \mathcal{G}^* (\tau_c \mathcal{G} - i \partial_\omega \mathcal{G})) / |\mathcal{G}| \quad (7)$$

defines the locations of saddle-node bifurcations in the (ω, N) -projection. The corresponding curves can again be traced numerically (dotted curves in Fig. 2). They separate the (ω, N) -projection into regions of unstable *antimodes* (grey shaded areas of Fig. 2) and possibly stable *modes*.

The saddle-node bifurcation curves determine possible boundaries of the CM stability region, even though they are independent of the carrier rate equation parameters.

² $\tilde{\phi}(\omega, N)$ is defined for a non-vanishing $|\mathcal{G}|$, *i.e.*, for those (ω, N) that are not the CW states of the solitary laser.

³To trace these curves one needs to find initial points (ω, N) , which we obtain by root finding by imposing that $\tilde{\zeta}$ and $\tilde{\phi}$ are satisfied at some fixed N but for a variable ω .

To complete the stability analysis one needs to check also the appearance of Hopf bifurcations. Now the parameters ε and J in the carrier rate equation are playing a role. However, for small ε and for moderate or high feedback the location of the most important Hopf bifurcation branches can be approximated by the positions in the (ω, N) -projection (or the (ϕ, ζ) -plane) at which a pair of CMs has the same threshold N ; see Refs. [7, 8, 9]. In the vicinity of these locations one of the CMs involved gains and another loses stability. The beating-type periodic orbits resulting from these bifurcations form connecting branches between both CMs, which are known as bridges between cavity modes in the LK system[10].

The condition of *equal threshold* is again independent of the carrier rate equation parameters and is given by two complex (four real) equations

$$0 = \mathcal{T}(\omega, N, \Delta, \zeta, \phi) \stackrel{def}{=} \begin{cases} \mathcal{G}(\omega, N) - \zeta e^{i\varphi} e^{-i\omega\tau_c} \\ \mathcal{G}(\omega + \Delta, N) - \zeta e^{i\varphi} e^{-i(\omega+\Delta)\tau_c} \end{cases} \quad (8)$$

relating the real factors N , ω , ζ , ϕ and the mode frequency difference Δ . Thus, solutions with equal threshold form curves in the (ω, N) -projection (dash-dotted curves in Figs. 2 and 4). Accordingly, in the (ω, N) -projection they (approximately) distinguish the regions of unstable (hatched area in Fig. 2) and stable *modes*. The (ω, N, ζ, ϕ) -location at which the mode separation vanishes ($\Delta = 0$) is determined by the pair of complex equations

$$\mathcal{G}(\omega, N) = \zeta e^{i\varphi} e^{-i\omega\tau_c}, \quad \partial_\omega \mathcal{G}(\omega, N) = -i\tau_c \zeta e^{i\varphi} e^{-i\omega\tau_c}.$$

In the TW model it is known as a *mode degeneracy* point.

Up to now we have considered an abstract laser response function \mathcal{G} . In the remainder of this section we derive the expressions for the response function \mathcal{G} and the factors ζ , ϕ for the LK model and for the TW model, respectively, which we distinguish by subscripts.

3.1 External cavity modes of the LK model

In the well-investigated LK model the CMs are better known as *external cavity modes* (ECMs). The function \mathcal{G} and the feedback factors ζ , ϕ from Eq. (5) can be defined by

$$\mathcal{G}_{LK}(\omega, N) \stackrel{def}{=} i\omega - (1 + i\alpha_H)N, \quad \zeta_{LK} \stackrel{def}{=} \eta, \quad \phi_{LK} \stackrel{def}{=} \psi. \quad (9)$$

These expressions can be obtained after inserting ansatz (4) into (1). A *unique* root $(\omega, N) = (0, 0)$ of the function \mathcal{G}_{LK} defines the CW state of the solitary laser, which has the field intensity $|E|^2 = J$.

Some level curves of the functions $\tilde{\zeta}_{LK}$ and $\tilde{\phi}_{LK}$ defined by Eq. (6) are represented by the solid and the dashed curves in Fig. 2(a). Open circles and black dots in this figure show *modes* and *antimodes* of the LK model for $\eta = 0.2$ and $\psi = 0$.

The dotted saddle-node curve separates the regions of *modes* and *antimodes*; it was found from condition (7). The dash-dotted curve is the equal-threshold curve that approximates Hopf bifurcations and, therefore, restricts the *mode* stability region (white area in Fig. 2(a)). The level curves of $\tilde{\zeta}_{LK}(\omega, N)$ (ellipses of ECMs), as well as solutions of Eqs. (7,8), can be given by the explicit expressions

$$\begin{aligned} \tilde{\zeta}_{LK}(\omega, N) = \eta &\Leftrightarrow \begin{cases} \omega = \eta(\alpha_H \sin(t) + \cos(t)) \\ N = \eta \sin(t) \end{cases}, \\ \mathcal{F}_{LK}(\omega, N) = 0 &\Leftrightarrow N = \frac{\alpha_H \omega + 1/\tau_c}{1 + \alpha_H^2}, \\ \mathcal{T}_{LK}(\omega, N, \Delta, \eta, \psi) = 0 &\Leftrightarrow \begin{cases} \omega = \frac{\Delta}{2} \left(\alpha_H \text{ctg} \left(\frac{\Delta \tau_c}{2} \right) - 1 \right) \\ N = \frac{\Delta}{2} \text{ctg} \left(\frac{\Delta \tau_c}{2} \right) \\ \eta = \left| \frac{\Delta}{2} \sin^{-1} \left(\frac{\Delta \tau_c}{2} \right) \right| \\ \psi = \frac{\alpha_H \Delta \tau_c}{2} \text{ctg} \left(\frac{\Delta \tau_c}{2} \right) + \pi \text{ceil} \left(\left| \frac{\Delta \tau_c}{2\pi} \right| \right) \pmod{2\pi} \end{cases}. \end{aligned}$$

The field intensity of each ECM is given by $|E_s|^2 = (J - N_s)/(2N_s + 1)$. It must be positive, so that only the ECMs with $N_s \leq J$ are physically relevant; see also Ref. [11].

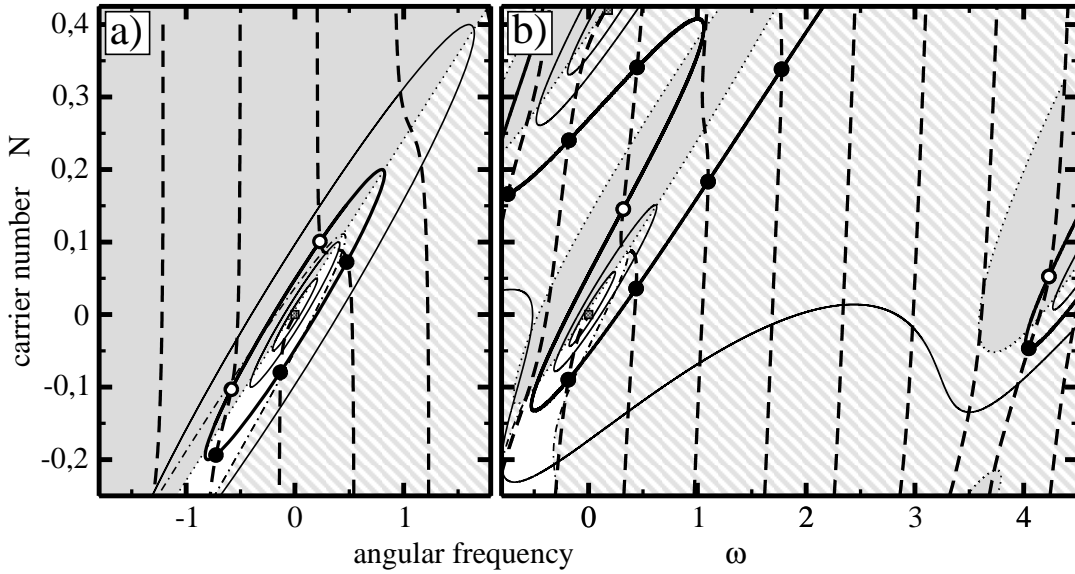


Figure 2: CMs in (ω, N) -projection for the LK model (a) and for the TW model (b). Solid curves: level curves of $\tilde{\zeta}(\omega, N)$ for $\zeta = 0.2$ (thick), 0.05 and 0.1 (thin inner), or 0.4 (thin outer). Dashed curves: level curves of $\tilde{\phi}(\omega, N)$ for $\phi = 0$. Dotted curves: saddle-node bifurcation curves. Dash-dotted curves: equal-threshold curves. Black dots and open circles: *modes* and *antimodes* at $\phi = 0$ and $\zeta = 0.2$. Squares: CW states of the solitary laser. Grey shading: regions of *antimodes*. Hatching: approximate region of unstable *modes*.

3.2 Compound cavity modes of the TW model

The TW model was used intensively to model the dynamics of multisection lasers with comparable lengths of the sections. The CMs are characterized by spatial distributions of the fields in all parts of the device. Thus, the CMs in the TW model case are due to both the internal laser cavity and the EC, and this is why they are called *compound cavity modes* (CCMs).

In the present case, the continuous wave amplitude E_s from Eq. (4) is given by a pair of complex time-independent functions $E_s^\pm(z)$ representing spatial distributions of the counterpropagating fields. The insertion of ansatz (4) into the boundary conditions and into the field equations of the TW model (3) yields

$$E_s^+(-l) = 0, \quad E_s^-(0) = rK e^{i\varphi} E_s^+(0) e^{-i\omega_s \tau_c}, \quad (10)$$

and the linear system of ODE's

$$\begin{aligned} \frac{d}{dz} \begin{pmatrix} E_s^+ \\ E_s^- \end{pmatrix} (z) &= \frac{1}{l} \begin{pmatrix} -(\xi_s - \xi_0) & -i\kappa \\ i\kappa & (\xi_s - \xi_0) \end{pmatrix} \begin{pmatrix} E_s^+ \\ E_s^- \end{pmatrix}, \quad z \in (-l, 0), \quad \text{which implies} \\ \begin{pmatrix} E_s^+ \\ E_s^- \end{pmatrix} (0) &= \frac{\sinh(\chi_s)}{\chi_s} \begin{pmatrix} \chi_s \coth(\chi_s) - (\xi_s - \xi_0) & -i\kappa \\ i\kappa & \chi_s \coth(\chi_s) + (\xi_s - \xi_0) \end{pmatrix} \begin{pmatrix} E_s^+ \\ E_s^- \end{pmatrix} (-l), \quad (11) \\ \xi_s &= \xi(\omega_s, N_s), \quad \chi_s = \sqrt{(\xi_s - \xi_0)^2 + \kappa^2}, \\ \xi(\omega, N) &\stackrel{def}{=} l(i\omega - (1 + i\alpha_H)N) = l\mathcal{G}_{LK}(\omega, N). \end{aligned}$$

The EC and the laser response functions can now be defined by the relations between the amplitudes $E_s^\pm(z)|_{z=0}$ (*i.e.*, the amplitudes for $z = 0$) that describe fields that are incoming into (or outgoing from) the EC and laser, respectively:

$$\begin{aligned} \text{EC: } E_s^-(0) &= \gamma \zeta_{TW} e^{i\phi_{TW}} e^{-i\omega_s \tau_c} E_s^+(0), \\ \zeta_{TW} &\stackrel{def}{=} |r|K/|\gamma|, \quad \phi_{TW} \stackrel{def}{=} \varphi + \arg(r/\gamma), \\ \text{laser: } E_s^-(0) &= \gamma \mathcal{G}_{TW}(\omega_s, N_s) E_s^+(0), \\ \mathcal{G}_{TW}(\xi(\omega, N)) &\stackrel{def}{=} \frac{i}{\gamma\kappa} \left(\frac{\sqrt{(\xi - \xi_0)^2 + \kappa^2}}{\tanh\left(\sqrt{(\xi - \xi_0)^2 + \kappa^2}\right)} + (\xi - \xi_0) \right), \\ \text{where } \gamma &\stackrel{def}{=} i\kappa l(1 - \xi_0)/(\xi_0^2 + \kappa^2). \end{aligned} \quad (12)$$

For all CW states (ω, N) of the solitary DFB laser with antireflection coatings the condition $\gamma \mathcal{G}_{TW}(\omega, N) = 0$ holds⁴. By a proper selection of the detuning and the reference carrier density factors δ and n_{ref} ⁵ we can always achieve that a pair $(\omega, N) = (0, 0)$ is a root of the function \mathcal{G}_{TW} , while $|\mathcal{G}_{TW}(\omega, N)|$ is strictly positive

⁴Only a finite number of the CCMs is given by roots (ω, N) of the function \mathcal{G}_{TW} satisfy the necessary condition $N < J$, which is implied by the non-negativeness of the mean photon number $\langle |E_s|^2 \rangle_L$.

⁵In our example we have chosen a nice value of n_{ref} and adjusted the absorption α instead (see Table 1).

for all $N < 0$. The complex factor γ defined in Eq. (12) scales the function $\mathcal{G}_{TW}(\xi)$, so that $\partial_\xi \mathcal{G}_{TW}|_{\xi=0} = 1/l$. This will be used when comparing the LK and the TW models in the next section.

We use the laser response function \mathcal{G}_{TW} from Eq. (12) to build the functions $\tilde{\zeta}_{TW}$ and $\tilde{\phi}_{TW}$ of Eq. (6), as well as the saddle-node function \mathcal{F}_{TW} of Eq. (7) and the equal-threshold function \mathcal{T}_{TW} of Eq. (8). The numerical continuation of the saddle-node condition, of the equal-threshold curves and of the level curves of $\tilde{\zeta}_{TW}$ and $\tilde{\phi}_{TW}$ is represented in Fig. 2(b). One can recognize the multimode nature of the TW model for the solitary laser in this figure. With decreasing feedback amplitude, the level curves of $\tilde{\zeta}_{TW}(\omega, N)$ are forming shrinking loops, which collapse at the CW states of the solitary laser. Each such set of closed loops should be compared with ECM ellipses of the LK model. Note also that the centers of these closed loops are not exactly at the solitary laser CW states. With an increase of the feedback these loops grow and collide with each other⁶, forming larger curves that bypass multiple CW states of the solitary laser. Thus, when tuning the feedback phase at larger feedback levels, one must expect an increasing difference between the ECMs of the LK model and the CCMs of the TW models.

4 Comparison between ECMs and CCMs

We now concentrate on the ECMs and CCMs that are located close to the CW state $(\omega, N) = (0, 0)$ of the solitary laser. In this case $|\mathcal{G}_{LK}(\omega, N)|$ is small and the function \mathcal{G}_{TW} can be given by its Taylor expansion

$$\begin{aligned} \mathcal{G}_{TW}(\xi(\omega, N)) &= \mathcal{G}_{TW}|_{\xi=0} + \partial_\xi \mathcal{G}_{TW}|_{\xi=0} \xi + \frac{1}{2} \partial_{\xi\xi} \mathcal{G}_{TW}|_{\xi=0} \xi^2 + \mathcal{O}(\xi^3) \\ &= \mathcal{G}_{LK}(\omega, N) + \gamma_2 \mathcal{G}_{LK}^2(\omega, N) + \mathcal{O}(\mathcal{G}_{LK}^3), \\ \text{where } \gamma_2 &\stackrel{\text{def}}{=} \frac{l^2}{2} \partial_{\xi\xi} \mathcal{G}_{TW}|_{\xi=0}. \end{aligned} \quad (13)$$

Accordingly, we obtain the following expressions for the functions $\tilde{\zeta}$ and $\tilde{\phi}$ from Eq. (6) in the TW and the LK models:

$$\begin{aligned} \tilde{\zeta}_{TW}(\omega, N) &= \tilde{\zeta}_{LK}(\omega, N) \cdot [|1 + \gamma_2 \mathcal{G}_{LK}(\omega, N)| + \mathcal{O}(|\mathcal{G}_{LK}|^2)], \\ \tilde{\phi}_{TW}(\omega, N) &= \tilde{\phi}_{LK}(\omega, N) + \arg(1 + \gamma_2 \mathcal{G}_{LK}(\omega, N)) + \mathcal{O}(|\mathcal{G}_{LK}|^2). \end{aligned} \quad (14)$$

The laser response ($\mathcal{G}_{TW}, \mathcal{G}_{LK}$), as well as the feedback amplitude ($\tilde{\zeta}_{TW}, \tilde{\zeta}_{LK}$) or phase ($\tilde{\phi}_{TW}, \tilde{\phi}_{LK}$) functions, coincide to first order. Thus, we should relate the feedback amplitude and phase parameters in the LK and the TW models as follows:

$$\eta = \zeta_{LK} \approx \zeta_{TW} = |r|K/|\gamma|, \quad \psi = \phi_{LK} \approx \phi_{TW} = \varphi + \arg(r/\gamma). \quad (15)$$

To have simple expressions between the feedback amplitudes ($K = 2\eta$) and between the feedback phases ($\varphi = \psi$), we have adjusted the amplitude and the argument of the facet reflectivity factor r in our example; see Table 1.

⁶The collision points (ω, N) can be found by solving the equations $\partial_\xi \mathcal{G}_{TW}(\bar{\xi}) = 0$, $\xi(\omega, N) = \bar{\xi}$.

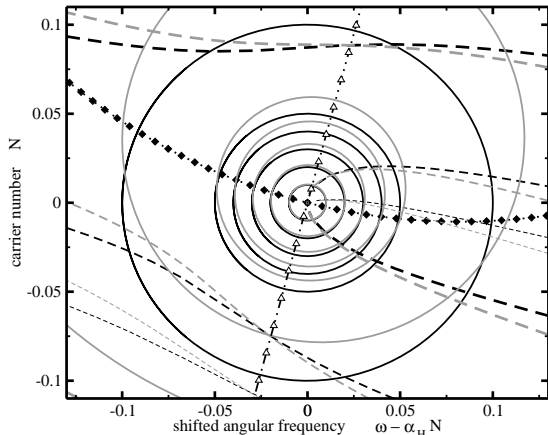


Figure 3: CMs in the vicinity of $(0, 0)$ in the LK model (black curves) and the TW model (grey curves). Solid curves (counting from inside): level curves of $\tilde{\zeta}(\omega, N)$ for $\zeta = \eta = K/2 = 0.01, 0.02, 0.03, 0.04, 0.05$ and 0.1 . Dashed curves: level curves of $\tilde{\phi}(\omega, N)$ for $\phi = \psi = \varphi = 0$ (thick), π (moderate) and 0.6π (thin). Triangles and rhombs: functions $\tilde{\phi}, \tilde{\zeta}$ in the TW and the LK models have a higher order coincidence. Cavity modes at fixed ζ and ϕ are given by the intersections of the corresponding solid and dashed curves.

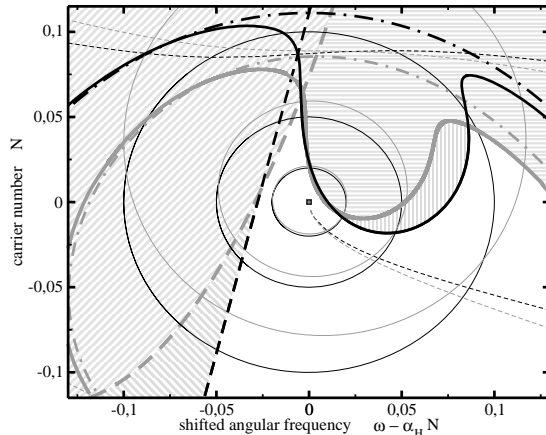


Figure 4: Bifurcations in the vicinity of $(\omega, N) = (0, 0)$ in the LK model (black curves) and in the TW model (grey curves). Thick dashed curve: saddle-node bifurcation. Thick solid curve: Hopf bifurcation. Dash-dotted curve: equal-threshold condition. Thin solid and dashed curve: some fixed feedback amplitude and fixed-phase curves as in Fig. 3. Slanted hatching: regions of *antimodes* (saddles). Vertical (horizontal) hatching: regions of unstable *modes* (nodes).

To compare different level curves of the two different models we plotted them both in Fig 3. We actually plot these curves as a function of $\omega - \alpha_H N$ to make the CM ellipses more visible. It can be checked that this representation transforms the ECM ellipses of the LK system into circles (black solid curves in Fig. 3). For smaller feedback amplitudes ($\zeta = 0.01$ or 0.02) the corresponding ellipses, as well as the fixed-phase curves (dashed curves), of both models are in rather good agreement. However, with an increase of ζ , the ECM loops (grey solid) as well as the fixed-phase curves (grey dashed) of the TW model are slightly out of place. The loops are shifted upwards, while the fixed-phase curves are slightly rotated clockwise. These changes are due to non-vanishing higher-order terms in Eq. (14). If the conditions

$$\begin{aligned}
 |1 + \gamma_2 \mathcal{G}_{LK}| = 1 &\Leftrightarrow \begin{cases} \omega = \Im m [(i\alpha_H - 1)(1 - e^{it})/\gamma_2] \\ N = \Re e [(1 - e^{it})/\gamma_2] \end{cases}, \quad \text{or} \\
 \arg(1 + \gamma_2 \mathcal{G}_{LK}) = 0 &\Leftrightarrow N = \frac{\Re e[\gamma_2] \omega}{\Im m[\gamma_2(1 + i\alpha_H)]}
 \end{aligned}$$

are satisfied then the next higher-order term of the function $\tilde{\zeta}_{TW}$ or $\tilde{\phi}_{TW}$ in Eq. (14) vanishes as well. The locations where this happens are indicated in Fig. 3 by filled rhombs and open triangles, respectively. The interpretation is that the correspond-

ing fixed CM ellipses (or the fixed-phase curves) of the TW and LK models cross each other approximately at these positions.

In Fig. 4 we also compared the saddle-node conditions and the equal-threshold curves defined by Eqs. (7) and (8). The saddle-node curve of the TW model (grey dashed) is rotated slightly as we have seen before for the fixed-phase curves. At the same time, the equal-threshold curve (grey dash-dotted) is shifted downwards, *i.e.*, in the opposite direction of the shift of the CM loops. The Hopf bifurcation curves, computed with the continuation package AUTO from the characteristic equation [12, 13], (thick solid) are also indicated, as are stability regions of the CMs (white areas).

5 Conclusions

We have compared the cavity modes of the laser with conventional optical feedback as modelled by the Lang-Kobayashi equations and by a traveling wave model. By deriving the scaling factor that relates the two models we showed good qualitative agreement, even at the moderate levels of feedback, between the external cavity modes of the LK model and the compound cavity modes of the TW model. For low levels of feedback we even found quantitative agreement.

Future work will include a more detailed comparison between the LK and TW models on the level of one-parameter and two-parameter bifurcation diagrams.

Acknowledgment

The work of M.R. was supported by DFG Research Center MATHEON “Mathematics for key technologies: Modelling, simulation, and optimization of real-world processes”.

References

- [1] R. Lang, and K. Kobayashi, ”External optical feedback effects on semiconductor injection properties”, *IEEE J. of Quant. El.*, **16**, pp. 347–355, 1980.
- [2] J.E. Carrol, J.E.A. Whiteaway, and R.G.S. Plumb, *Distributed Feedback Semiconductor Lasers*, IEEE Publishing, 1998.
- [3] U. Bandelow, M. Radziunas, J. Sieber, and M. Wolfrum: “Impact of gain dispersion on the spatio-temporal dynamics of multisection lasers”, *IEEE J. Quantum Elect.*, **37**, pp. 183–188, 2001.

- [4] B. Krauskopf, "Bifurcation analysis of lasers with delay", in *Unlocking Dynamical Diversity: Optical Feedback Effects on Semiconductor Lasers*, D.M. Kane and K.A. Shore, ed., pp. 147–183, Wiley, 2005.
- [5] T. Heil, I. Fisher, W. Elsässer, B. Krauskopf, K. Green, and A. Gavrielides, "Delay dynamics of semiconductor lasers with short external-cavity laser diodes: Bifurcation scenarios and mechanisms", *Phys. Rev. E*, **67**, 066214, 2003.
- [6] O. Ushakov, S. Bauer, O. Brox, H.-J. Wünsche, and F. Henneberger, "Self-organization in semiconductor lasers with ultra-short optical feedback", *Phys. Rev. Lett.* **92**, 043902, 2004.
- [7] O. Brox, S. Bauer, M. Radziunas, M. Wolfrum, J. Sieber, J. Kreissl, B. Sartorius, H.-J. Wünsche, "High-frequency pulsations in DFB-lasers with amplified feedback", *IEEE J Quantum Elect.*, **39**, pp. 1381-1387, 2003.
- [8] A. Tager, K. Petermann, "High frequency oscillations and self-mode locking in short external cavity laser diodes", *IEEE J Quantum Elect.*, **30**, pp. 1553-1561, 1994.
- [9] M. Wolfrum, D. Turaev: "Instabilities of lasers with moderately delayed optical feedback", *Optics Communications*, **212**, pp. 127-138, 2002.
- [10] T. Erneux, F. Rogister, A. Gavrielides, V. Kovanis, "Bifurcations to mixed external cavity mode solutions for semiconductor lasers subject to optical feedback", *Optics Communications*, **183**, pp. 476-477, 2000.
- [11] V. Rottschäfer and B. Krauskopf, "The ECM-backbone of the Lang-Kobayashi equations: a geometric picture", Applied Nonlinear Mathematics Research Report **2005.20**, University of Bristol.
- [12] E.J. Doedel, A.R. Champneys, T.F. Fairgrieve, Yu.A. Kuznetsov, B. Sandstede, and X. Wang, "AUTO97: Continuation and bifurcation software for ordinary differential equations (with HomCont)", *Technical report*, Concordia University, 1997.
- [13] M. Radziunas, "Numerical bifurcation analysis of the traveling wave model of multisection semiconductor lasers", *Physica D*, **213**, pp. 98–112, 2006.